**NUCLEAR
INSTRUMENTS
& METHODS
IN PHYSICS
RESEARCH**
Section A

A silicon imaging calorimeter prototype for antimatter search in space: experimental results

M. Bocciolini, F. Celletti, A. Perego and P. Spillantini

Dipartimento di Fisica dell'Università di Firenze and Sezione INFN di Firenze, Firenze, Italy

G. Basini, F. Bongiorno [1], F. Massimo Brancaccio and M. Ricci

Laboratori Nazionali di Frascati dell'INFN, Frascati, Italy

M.T. Brunetti, A. Codino, M. Menichelli, M. Miozza and I. Salvatori

Dipartimento di Fisica dell'Università di Perugia and Sezione INFN di Perugia, Perugia, Italy

V. Bidoli, M. Candusso, C. De Fabritiis, M.P. De Pascale, A. Morselli and P. Picozza

Dipartimento di Fisica dell'Università "Tor Vergata", Roma and Sezione INFN di Roma II, Roma, Italy

A. Buccheri, A. Incicchitti and D. Prosperi

Dipartimento di Fisica dell'Università "La Sapienza", Roma and Sezione INFN di Roma, Roma, Italy

G. Barbiellini, M. Boezio, F. Fratnik, P. Schiavon, A. Vacchi and N. Zampa

Dipartimento di Fisica dell'Università di Trieste and Sezione INFN di Trieste, Trieste, Italy

This report presents the results obtained with a prototype silicon–tungsten (Si–W) electromagnetic calorimeter, conceived as a fine-grained imaging device to carry out studies of the antimatter component in primary cosmic radiation. The calorimeter prototype contains 20 x, y sampling layers interleaved with 19 showering material planes. One sensitive layer is obtained with two silicon strip detectors (Si-D) (60×60) mm^2, each divided into 16 strips, 3.6 mm wide; the two detectors are assembled back to back with perpendicular strips. This allows the transverse distributions of the shower in both coordinates at each sampling ($0.5\ X_0$) to be pictured. The basic characteristics of the design and the experimental results obtained on a test beam at the CERN proton synchrotron (PS) for electrons and pions are reported. The main results presented are the response of the calorimeter to the electron at various energies (1–7 GeV), and the transverse shower profiles at different calorimeter depths as well as the patterns of the electromagnetic shower and those of the interacting and non-interacting pions. The capability of the calorimeter in measuring the direction of the incoming electromagnetic particle from the pattern of the shower has been evaluated at different energies. These results are encouraging in view of the possible use of this detector to search for high-energy γ sources in space.

1. Introduction

The detector is a prototype of the electromagnetic calorimeter conceived for the WiZard [1] experiment to investigate, in a planned space mission, the antimatter component in primary cosmic radiation. Beside the calorimeter, the WiZard apparatus is composed of a momentum analyser superconducting magnet with drift chamber tracking, a transition radiation detector, and a time-of-flight system.

Minimum ionizing particles (mip) produce about 80 electron–hole pairs per μm of Si-D crossed; the corresponding charge collection is a process not subject to instabilities or nonlinear effects. The segmentation of each Si-D provides the calorimeter with a high spatial granularity. The shower profile is measured at each sampling plane in both the x and y coordinates.

The allowed weight for the mentioned space applications limits the calorimeter depth to about 10 X_0, which is insufficient for the full energy containment of

---

[1] Also at Dipartimento di Metodi e Modelli Matematici dell'Università 'La Sapienza', Roma, Italy.

high-energy electromagnetic particles. The high granularity and energy resolution of the silicon detectors makes them capable of measuring the shower profiles and the tracks of the particles with high accuracy [2], thus allowing good particle identification also in the absence of the full shower containment.

Experimental data from calorimeters based on silicon as an active material have already been published [3–7]. In the present paper more evidence is given about the results concerning their high segmentation and shower-imaging capability; beside its characteristics as a particle identifier, the calorimeter achieves good accuracy (a few mrad) in reconstructing the direction of the incoming particle. This prototype calorimeter is the first constructed with detectors having an area of (60×60) mm^2. The detectors are kept in special packages which, when patched together to form large surfaces, allow a minimal dead area for the sampling planes of the calorimeter.

The Si–W calorimeter can play a decisive role in the event definition, especially in the search for antimatter in cosmic radiation. Moreover, the data from the first few planes of this calorimeter can be considered as a source of information for the design of a preshower detector.

2. The tracking calorimeter

The calorimeter prototype, whose characteristics are given in table 1, consists of 20 layers of silicon detectors [1] alternated with 19 planes of tungsten. The thickness of the material crossed by the incident beam before the first sensitive layer corresponds to 0.2 X_0.

In the design of this prototype we were bound by the constraints, common to all experiments in space, of limited weight, low power consumption, and high reliability. In addition, structural constraints affect the geometrical parameter of the calorimeter and, in particular, the distance between the sensitive planes. The transverse granularity was chosen for the aims of the WiZard apparatus through Monte Carlo (MC) calculations [2]. One sensitive element is composed of two Si detectors mounted back to back with an on-line pin structure and perpendicular strips to give x and y coordinates as shown in fig. 1; for the Si-D this allows the use of a well-established technology suitable for highly automatized mass production and low costs. The dead area, which is due to the wire bonding to the ceramic support, is less than 2%.

The general characteristics of one Si-D are listed in table 2. All the Si-Ds used in this prototype are anal-

---

Table 1
Si–W prototype calorimeter characteristics

Active area	59×59 mm^2
Number of Si-D x, y sampling	20
Number of tungsten plates	19
Thickness of the Si-D per sampling	2×380 μm
Thickness of the tungsten plates	1.75 mm (0.5 X_0)
Total depth (W)	9.5 X_0
Pitch of the stripes on the Si-D	3.6 mm
Distance between sampling layers	24.5 mm
Working voltage (> full depletion)	80 V
Number of electronic channels	640
Power dissipation per channel	15 mW

---

ysed before, during, and after the packaging procedure, and the parameters of each strip are stored in a data base available for studies of radiation resistance and long-term stability. Each detector assembly is mounted on a multilayer board, which also carries the front-end electronics and the related wiring. The calorimeter prototype is contained in an aluminium box, which has one of its side walls made of a multilayer board to provide the connections of the detector's card to the outside electronics.

The design of the readout electronics has been specifically developed to take into account the future application of the calorimeter in space research. It has been conceived for low-power consumption (15 mW per channel) and low electronic noise, i.e. ≤ 2700 electrons rms for 1000 pF input capacitance, the shaping time being 7 μs. In the final version of the calorimeter the strips of each detector will be connected to the neighbouring one to form single strips 48 cm long. Two full-scale outputs are available and give, for an Si-D of 380 μm thickness, a linear response up
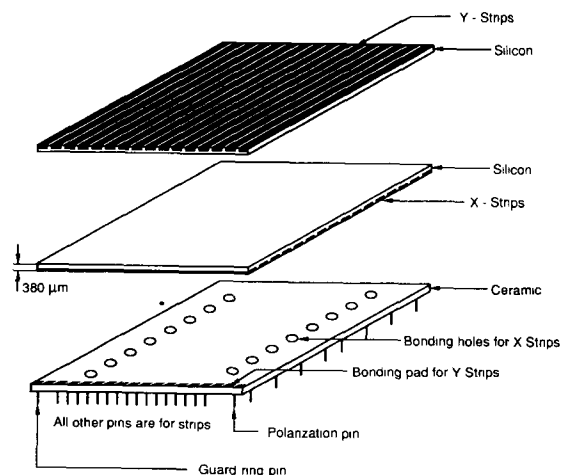

Fig. 1. Schematic view of the packaging of two detectors with perpendicular strips.

Table 2
Si-D characteristics

Total area	(60×60) mm^2
Number of strips	16
Thickness	(380 ± 15) μm
Strip pitch	3.6 mm
Crystal	n-type, (FZ) Si, $R \geq 4$ kΩ cm
Readout coupling	ohmic
Strip capacitance	≈ 70 pF

to 25 or 400 mip, respectively. This range covers the very large dynamics required in the calorimeter. The readout is performed by means of a multiplexing system at a maximal frequency of 1 MHz.

An analog fast timing-out bipolar signal allows the auto-triggering based on the amount of energy released in a given section of the calorimeter.

3. Data taking

The prototype of the WiZard Si–W imaging calorimeter has been exposed to the PS test beam t_7 at CERN, where a magnetic channel can select negative or positive charged particles of momentum between 1 and 7 GeV/c, $\Delta p / p = \pm 1\%$. The dimension of the beam spot at the calorimeter entrance was 1 cm diameter as defined by a counters telescope. A pair of Cherenkov counters provided the identification of electrons and pions. Data have been collected in different runs at five beam energies between 1 and 7 GeV.

Data from the front-end electronics have been recorded by a standard acquisition system, allowing the storage of a complete event, and have been transferred via a VME-bus to a microcomputer system (VALET-PLUS) for recording and on-line monitoring.

Dedicated pion calibration runs at 4 GeV were performed to establish the energy scale for each strip.
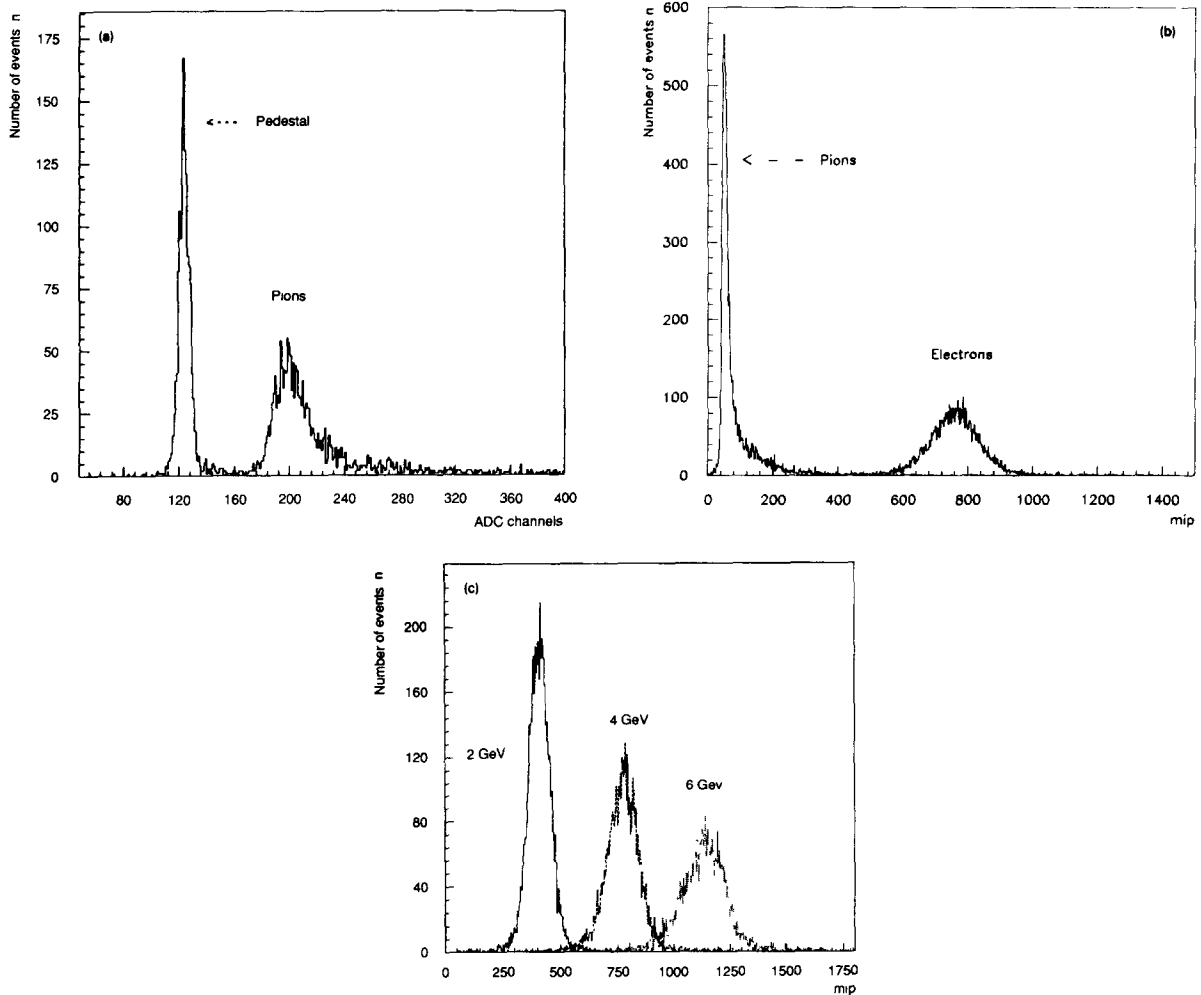

Fig. 2. (a) Energy distribution for 4 GeV pions crossing a single Si-D. (b) Total energy distribution for 4 GeV pions and electrons; (c) total energy distribution for 2, 4, and 6 GeV electrons.

The distance between the pedestal and the peak of the Landau distribution was taken as the energy unit (1 mip).

The calibration matrix has been measured strip by strip moving the prototype in the two transverse directions with respect to the beam by means of a remote-controlled mechanical support.

4. Experimental results and simulation

4.1. Energy response

The total energy contained in each single sampling layer or in the whole detector is found by adding the charge seen by all channels having an energy content above a threshold of 0.7 mip. About 5% of the strips were damaged and their energy content was deduced from the adjacent strips. We observed a capacitive coupling between the channels (2–3%); hence we used a correction based on the measured mean position of the pedestals during the runs with electrons.

The Monte Carlo simulation of the detector has been obtained with the GEANT code version 3.15. In analogy with the data analysis procedure, the energy scale has been calibrated with 4 GeV pions. We chose the explicit delta ray generation to simulate the fluctuations in the energy deposit. The cuts for the lowest energy were set at 10 keV for both photons and electrons.

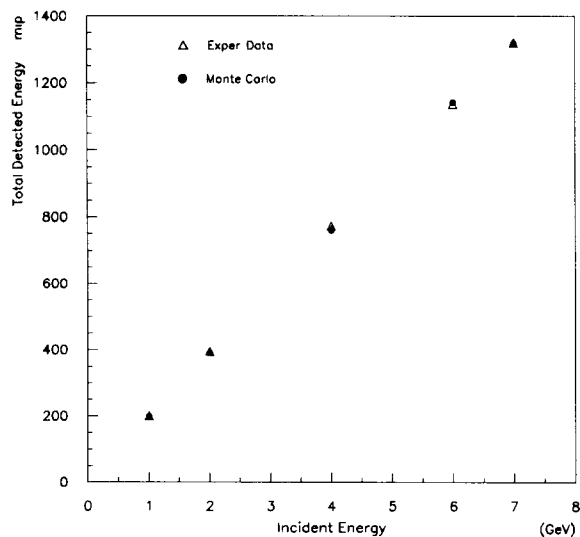The transverse and longitudinal energy containments for the prototype at these energies, as obtained

Table 3
Monte Carlo calculated transverse and longitudinal containment of the prototype tower for sampling steps of 0.5 X_0

E_{inc} [GeV]	Containment		
	Longitudinal	Transversal [% of E_{inc}]	Total [% E_{inc}]
1	96.0	63.9	60.0
2	93.2	65.8	59.0
4	89.7	67.7	57.4
6	87.6	68.5	56.2
7	86.1	69.4	55.5

from the MC calculation, can be deduced from table 3 where the respective percentage of containment is given.

The typical response of the strips to pions is given in fig. 2a, where the distribution of the mip energy loss is given in units of analog-to-digital converter (ADC) channels. From this figure it is also possible to evaluate a signal-to-noise ratio of better than 20, with an input capacitance of 80 pF. Fig. 2b shows the distributions of detected energy for pions and electrons at 4 GeV, whilst fig. 2c gives the distribution of the deposited energy for electrons at 2, 4, and 6 GeV.

The total charge released in the calorimeter by electrons at different energies (expressed in mip units) is given in fig. 3 together with data from MC simulation (if the errors, here and in the following, are not shown they are contained in the graphic points). The response of the calorimeter, in this energy range, shows a quasi-linear behaviour with deviations accounting for the partial containment at different energies (see table 3).

Fig. 4 shows the relative energy resolution versus $1/\sqrt{E}$ for the measured energies compared with MC simulation. The data are divided by the square root of the sampling step expressed in units of radiation length $\sigma(E)/(E\sqrt{t})$, $t = 0.5$ X_0. The two MC simulations also shown refer to sampling steps $t = 0.5$ X_0 and $t = 1$ X_0; this last indicates the potential performance of the calorimeter for full containment.

4.2. Shower shape and shower direction measurement

The total energy released by the electron shower is measured with a fine transverse and longitudinal segmentation. The longitudinal segmentation allows the identification of the position of the shower maximum along its axis. On the other hand, the two transverse coordinates of the shower axis can be derived from the centre of gravity of the x, y transverse energy distributions at each sampling plane.

Fig. 5 shows the longitudinal development (experimental and simulated) of the showers initiated by 6

Fig. 3. Energy response of the calorimeter. The collected total mean charge is given in mip units as a function of the particle energy.
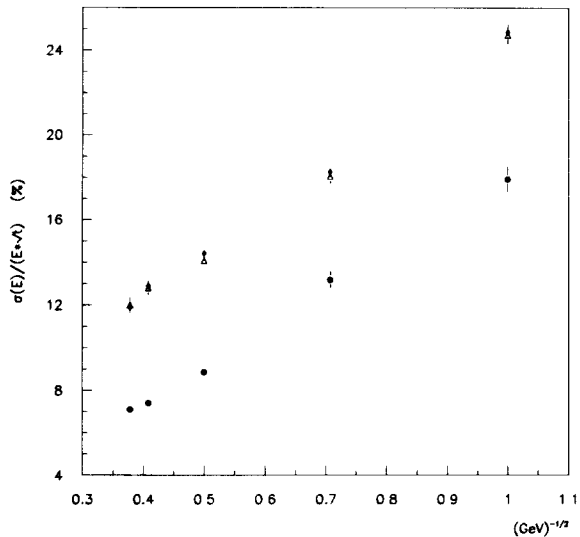
Fig. 4. Energy resolution data plotted against $1/\sqrt{E}$. The data are divided by the square root of the sampling step in units of radiation length, $\sigma(E)/(E\sqrt{t})$. The two MC simulations also reported refer to sampling steps $t = 0.5\ X_0$ and $t = 1\ X_0$; this last simulation shows the potential performance of the calorimeter for full containment. $\Diamond$ tower calorimeter experimental data (9.5 X_0); $\triangle$ tower calorimeter Monte Carlo data (9.5 X_0); $\bullet$ Monte Carlo data (19 X_0).

GeV electrons; the energy released is sampled over the 20 x, y sensitive planes.

Fig. 6 shows simultaneously the longitudinal and the transverse energy distributions for 2 GeV electrons as seen from the y detectors only.
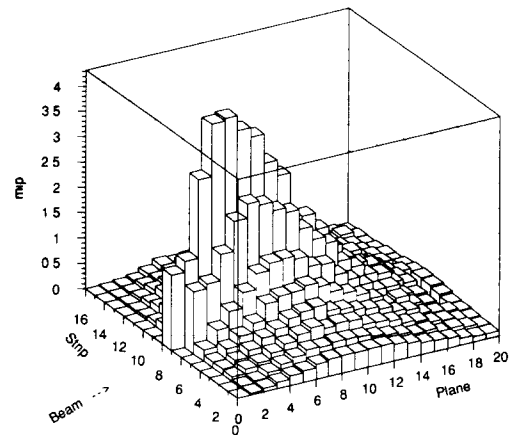

Fig. 6. Three-dimensional plot of the longitudinal and transverse energy distributions for 2 GeV electrons.

From the centres of gravity of the transverse shower profiles measured at different depth in the calorimeter we have derived the direction of the incoming particle. This direction is given by the linear fit connecting the centres of gravity of the transverse shower profiles obtained for each sampling. The center of gravity position has been evaluated for each event and weighted by the square root of the deposited energy; as an error on this position we have taken the width of the transverse distribution averaged over all events.

The mean value of the distributions of the slopes of these lines gives the direction of the beam. The σ value indicates the angular resolution of the imaging calorimeter. This σ value is shown for the two views in

Fig. 5. Longitudinal development (experimental and simulated) of a 6 GeV electron shower. The energy is sampled in 20 sensitive planes.
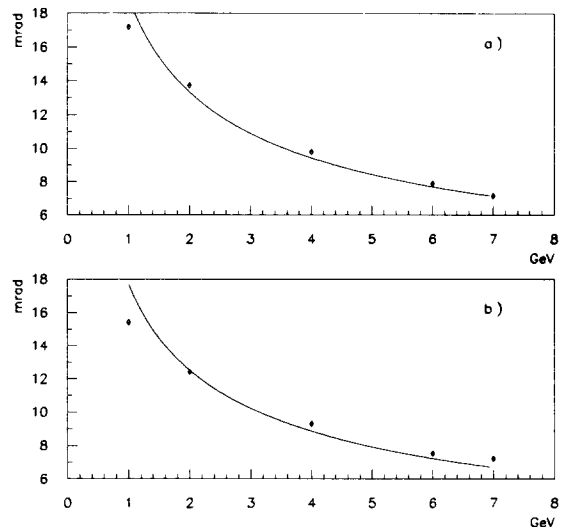

Fig. 7. The angular resolution of the imaging calorimeter is shown for the two views x and y as a function of the energy of the incoming electrons; the line corresponds to a $1/\sqrt{E}$ fit.
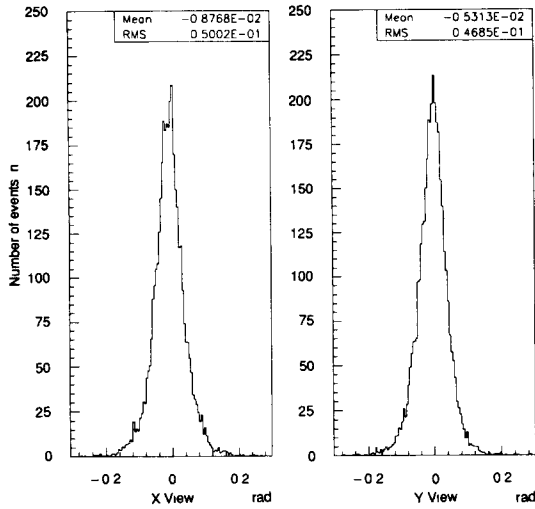
Fig. 8. Angular spread of the 4 GeV electrons shower axis as derived from the centres of gravity of the transverse shower profile in the first four contiguous sampling planes.

figs. 7a and 7b as a function of the energy of the incoming electrons. As expected, the angular resolution improves with growing energy like the relative resolution in the energy measurement.

The same algorithm has been applied to the first four calorimeter planes. The angular spread of the particles' directions so derived is shown in fig. 8 for 4 GeV electrons. Assuming the normal incidence of the original particle, the σ value of the distribution of the slopes represents the capability of the first four planes of the calorimeter in reconstructing the direction of the

impinging particles. This is relevant for the application of similar structures as a preshower detector.

With the aim of evaluating the capability of a single sampling plane of the calorimeter to identify the shower axis, we have taken as a reference the axis determined by all the sampling (excluding the one under analysis). The distribution of the differences between the shower–axis reference position and the position obtained from one single sampling plane indicates for that sampling plane the shower position reconstruction capability. In figs. 9a and 9b the widths of these distributions are reported as function of energy at two different depths in the calorimeter. Also in this case the $1/\sqrt{E}$ behaviour of the position resolution is evident.

4.3. Event pattern

The Si–W tracking calorimeter also reconstructs the event pattern, giving further information about the nature of the interacting particle. Some examples of event reconstruction for 4 GeV/c momentum particles are shown in figs. 10a and 10b, where the difference between the pattern of the shower induced by electrons and pions is clearly visible. By sampling the x and y shape of the shower development at each sensitive plane $(0.5\ X_0)$ the tracking calorimeter achieves a high power of discrimination between electrons and hadrons.

5. Conclusions

Tests on the tower prototype of the silicon tracking calorimeter have shown the capacity of this instrument
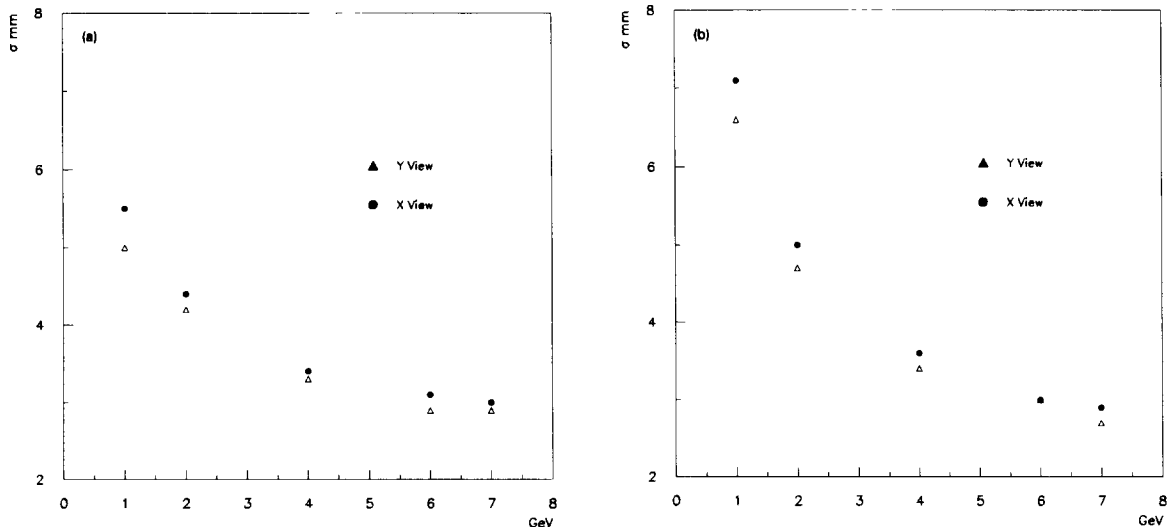

Fig. 9. Widths of the distributions of the differences between the shower–axis reference position and the position obtained from one single sampling plane reported as function of energy at two different depths in the calorimeter: (a) after 2 X_0 and (b) after 4 X_0.
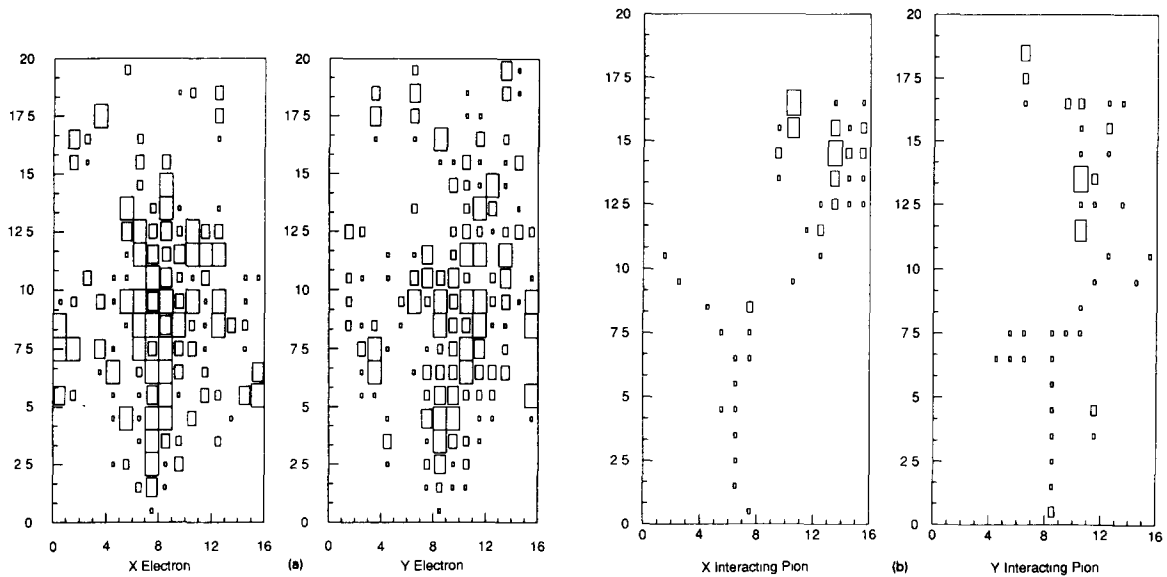
Fig. 10. Examples of pattern reconstruction for 4 GeV/c particles: (a) electromagnetic shower; (b) interacting pion. The size of the squares represents the amount of energy released in each strip.

to give detailed information on the shape of the shower development, combining the good resolution of the calorimeter and its high granularity. This allows identification of differently interacting particles, as required in the antimatter space research programme. The calorimeter can measure the direction of the photon-induced shower with an accuracy of a few mrad and can be used as a directional detector in the search for γ-rays pointlike sources in space.

The adequacy of the first part of this calorimeter as a preshower has also been proved experimentally.

Acknowledgements

References

[1] R.L. Golden et al., Nuovo Cimento B105 (1990) 191.
[2] M. Meschini et al., Nuovo Cimento B102 (1988) 523.
[3] G. Barbiellini et al., Nucl. Instr. and Meth. A257 (1987) 543.
[4] P.G. Rancoita and A. Seidman, Nucl. Instr. and Meth. A263 (1988) 84.
[5] S. Pensotti et al., Nucl. Instr. and Meth. A265 (1988) 266.
[6] S. Pensotti et al., Nucl. Instr. and Meth. A270 (1988) 327.
[7] A.L.S. Angelis et al., preprint CERN-EP/90-73 (1990).